Scattering functions of knotted ring polymers

Miyuki K. Shimamura,* Kumiko Kamata,† and Akihisa Yao‡
Graduate School of Humanities and Sciences, Ochanomizu University, 2-1-1 Ohtsuka, Bunkyo-ku, Tokyo 112-8610, Japan

Tetsuo Deguchi§
Department of Physics, Ochanomizu University, 2-1-1 Ohtsuka, Bunkyo-ku, Tokyo 112-8610, Japan
(Received 5 April 2005; revised manuscript received 10 August 2005; published 14 October 2005)

We discuss the scattering function of a Gaussian random polygon with N nodes under a given topological constraint through simulation. We evaluate the form factor $P_K(q)$ of a Gaussian polygon of $N=200$ having a fixed knot K for some different knots such as the trivial, trefoil, and figure-eight knots. Here the Gaussian polygons with different knots K have distinct values of the mean-square radius of gyration, $R^2_{G,K}$. We obtain the Kratky plots of the form factors—i.e., the plots of $(qR_{G,K})^2P_K(q)$ versus $qR_{G,K}$—for the different topological constraints and discuss nontrivial large-q behavior as well as small-q behavior for the scattering functions. We also find that the distinct values of $R^2_{G,K}$ play an important role in the large-q and small-q properties of the Kratky plots.

DOI: 10.1103/PhysRevE.72.041804 PACS number(s): 82.35.Lr, 05.40.Fb, 05.20.−y

I. INTRODUCTION

Ring polymers have attracted much interest in polymer physics, and their properties have been studied both theoretically and experimentally [1–6]. For the Gaussian random polygon the analytic expression of the static structure factor was obtained by Casassa [1]. The scattering function is compared with that of star polymers with four or five arms through the Kratky plot [1,5]. The scattering data of cyclic polystyrene in deuteriated cyclohexane at the θ temperature were obtained by the SANS experiment [6].

Recently statistical properties of ring polymers under topological constraints have been investigated extensively mainly through computer simulation [7–15]. It is first conjectured by des Cloizeaux that a topological constraint should lead to effective repulsion among segments of ring polymers so that the mean size of very long ring polymers should increase under topological constraints [7]. The conjecture is supported by several numerical observations [8,10–15]. In fact, the effective swelling due to topological constraints occurs particularly for ring polymers with small or zero excluded volume [14,15].

In this paper we discuss the scattering function of ring polymers under a topological constraint. It should be fundamental for studying ring polymers in scattering experiments. We consider ring polymers in solution at the θ temperature, and they are modeled by random polygons. Here, random polygons have no excluded volume—i.e., no thickness. We shall evaluate the radial distribution function in simulation and then take the Fourier transformation. We shall explicitly discuss the scattering function of a random polygon having some fixed knot type, making use of the Kratky plot of the form factor.

Let us introduce the Kratky plot for a linear polymer consisting of N segments. We first define the segment pair correlation function for the polymer by [16]

$$g(\boldsymbol{r}) = \frac{1}{N}\sum_{m,n=1}^{N} \langle \delta(\boldsymbol{r} - (\boldsymbol{R}_m - \boldsymbol{R}_n))\rangle. \tag{1}$$

Here $\boldsymbol{R}_m$ denotes the position vector of the mth segment of the polymer for $m=1,2,\ldots,N$. The (single-chain) static structure factor $g(\boldsymbol{q})$ of the polymer is defined by the Fourier transform of the pair correlation function as [16]

$$g(\boldsymbol{q}) = \int d\boldsymbol{r} e^{i\boldsymbol{q}\cdot\boldsymbol{r}} g(\boldsymbol{r}) = \frac{1}{N}\sum_{m,n=1}^{N} \langle \exp[i\boldsymbol{q}\cdot(\boldsymbol{R}_m - \boldsymbol{R}_n)]\rangle. \tag{2}$$

We also call it the scattering function. We define a form factor $P(\boldsymbol{q})$ as follows:

$$P(\boldsymbol{q}) = \frac{g(\boldsymbol{q})}{g(0)}. \tag{3}$$

Due to the rotational symmetry, the form factor is given by a function of $q=|\boldsymbol{q}|$ as follows:

$$P(\boldsymbol{q}) = f(qR_G). \tag{4}$$

Here R_G denotes the square root of the mean-square radius of gyration of the polymer: $R_G=\sqrt{\langle R_G^2\rangle}$. For such models of polymers with no excluded volume, the form factor has the large-q asymptotic behavior: $f(qR_G)\propto(qR_G)^{-2}$. Thus, it is useful to make the plot of $(qR_G)^2f(qR_G)$ versus qR_G. We call such a plot the *Kratky plot* of the form factor of the linear polymer [17].

There are several interesting simulation researches associated with topological effects of ring polymers [18–21]. For instance, the lengths of localized knots in self-voiding polygons have been extensively studied through a Monte Carlo

*Electronic address: miyuki@degway.phys.ocha.ac.jp
†Present address: Institute of Industrial Science, University of Tokyo, Meguro-ku, Tokyo 153–8505, Japan. Electronic address: kamakama@degway.phys.ocha.ac.jp
‡Electronic address: yao@degway.phys.ocha.ac.jp
§Electronic address: deguchi@phys.ocha.ac.jp

simulation of a lattice [18]. Here it is suggested that knots are localized in a knotted random polygon although the degree of localization should be rather weak. However, there has been no explicit numerical research on scattering functions of random polygons under different topological constraints.

Let us now review some known results on the influence of topological constraints on the average size of ring polymers with excluded volume. The average size is determined through competition among excluded-volume effects, finite-size effects, and topological effects [22]. In fact, such competition has been extensively studied in the simulation [15] of ring polymers consisting of cylindrical segments of radius δ. Here we note that the cylindrical model of self-avoiding polygons describes the statistical properties of DNA knots [23]. Let us denote by $\langle R^2_{G,K}(\delta)\rangle$ or simply by $R^2_{G,K}(\delta)$ the mean-square radius of gyration for such polygons that consist of N cylindrical segments of radius δ and have a given topology K; we denote by the symbol $\langle R^2_{G,all}(\delta)\rangle$ those of no topological constraint. We first discuss the large-N behavior. It has been shown numerically [15] that if the excluded-volume parameter δ is small, the mean-square radius of gyration of ring polymers with a fixed knot K is larger than that of no topological constraint for very large N; i.e., we have

$$R^2_{G,K}(\delta)/R^2_{G,all}(\delta) > 1 \quad \text{for } N \gg 1. \tag{5}$$

When the above ratio is larger than 1, we say that topological swelling occurs. If δ is greater than some value δ^*, however, the ratio becomes 1 when N is very large; i.e. there is no topological swelling.

The topological swelling leads to the nontrivial amplitude ratio when N is asymptotically large. The data of $\langle R^2_{G,K}(\delta)\rangle$ versus N for large values of N are well approximated by the asymptotic expansion in the following [15]:

$$R^2_{G,K}(\delta) = A_K N^{2\nu}\left[1 + B_K N^{-\Delta} + O(1/N)\right]. \tag{6}$$

Here ν is given by the exponent of self-avoiding walks, ν_{SAW}. For any given knot type K, the amplitude ratio $A_K/A_{all} > 1$ when $\delta < \delta^*$. Thus, the amplitude ratio is nontrivial for the case of thin ring polymers. In the case of $\delta > \delta^*$, however, the amplitude ratio is trivial: $A_K/A_{all} = 1$, which is consistent with the simulation results of self-avoiding polygons on lattices [24,25]. The numerical result is consistent with a phenomenological theory using two numbers expressing the excluded-volume and topological effects, respectively [15,26,27].

The typical finite-size behavior of cylindrical ring polymers is given as follows. For the trivial knot $K=0$, the ratio $R^2_{G,0}(\delta)/R^2_{G,all}(\delta)$ is equal to 1 for very small N, and it increases with respect to N and approaches some value larger than 1 when δ is small ($\delta < \delta^*$), while it is always equal to 1 when δ is large ($\delta > \delta^*$). For any nontrivial knot K, the ratio $R^2_{G,K}(\delta)/R^2_{G,all}(\delta)$ is smaller than 1 for small N; however, it increases with respect to N, and it becomes larger than 1 when δ is small ($\delta < \delta^*$), while it increases up to 1 when δ is large ($\delta > \delta^*$).

Let us next discuss the case of ideal ring polymers. It is shown by several simulation studies [10–13] that topological swelling indeed occurs for random polygons. Here we recall that ideal ring polymers and random polygons have no excluded volume. Furthermore, some schemes of asymptotic expansion have been discussed for the mean-square radius of gyration for random polygons under a topological constraint [10–13]. As far as the mean-square radius of gyration is concerned, it seems as if the topological effect might play a similar role as excluded volume. However, it does not give precisely the same effect. In fact, the distribution of the distance between opposite nodes of a random polygon with fixed knot is roughly described by the Gaussian one rather than that of self-avoiding walks [28]. Thus, also from this viewpoint, it should be nontrivial to study the scattering function of a random polygon under a topological constraint.

We discuss simulation results on the Gaussian random polygon in this paper—i.e., a model of ideal ring polymers. However, the numerical results of scattering functions should also be useful for scattering experiments of thin ring polymers with small excluded volume. In fact, as far as finite-size properties are concerned, simulation results of ideal ring polymers should be similar to those of thin ring polymers, as was the case of cylindrical ring polymers with very small radius δ [15]. Here we do not consider any asymptotic property such as the exponent ν of the gyration radius.

The contents of the paper are given as follows. In Sec. II we briefly discuss simulation methods. Then, we present the data of the mean-square radius of gyration, $\langle R^2_{G,K}\rangle$, for some topological conditions K, which are obtained for 10^5 Gaussian random polygons with $N=200$. In Sec. III we discuss the plot of the radial distribution function—i.e., the probability distribution $4\pi r^2 g_K(r)$ of the Gaussian polygons for different topological conditions K. We show that for each graph the peak position is located at the value of the square root of $\langle R^2_{G,K}\rangle$. In Sec. IV we discuss the scattering functions of the Gaussian polygons with the different topologies. In particular, we discuss the small-q and large-q behaviors of the scattering functions through the Kratky plot. In summary, we have evaluated the scattering functions of Gaussian random polygons with $N=200$ under some different topological conditions K. The Kratky plots have been obtained for the different K. They overlap up to $u=2$, they become separate for $u>2$, and they approach constant values for $u \gg 1$. The characteristic properties in the small- or large-q regions are explained in terms of the different values of the gyration radius $R_{G,K}$.

II. SIMULATION METHODS AND THE DATA OF THE MEAN-SQUARE GYRATION RADIUS

Making use of the conditional probability distribution [29], we have systematically constructed 10^5 samples of the Gaussian random polygon with 200 nodes. We have calculated two knot invariants $\Delta_K(-1)$ and $v_2(K)$ to each of the 10^5 configurations and effectively classified them into different topological classes. Here the symbol $\Delta_K(-1)$ denotes the determinant of a knot K, which is given by the Alexander polynomial $\Delta(t)$ evaluated at $t=-1$. The symbol $v_2(K)$ is the

TABLE I. Mean-square radius of gyration $\langle R^2_{G,K}\rangle$ and the fraction of a Gaussian random polygon with a topological condition K. Here $N=200$.

K	$\langle R^2_{G,K}\rangle$ (errors)	Fractions (errors)
0	18.033 (0.082)	0.533 (0.002)
3_1	16.208 (0.120)	0.214 (0.001)
4_1	15.043 (0.250)	0.045 (0.0006)
Other	13.459 (0.118)	0.188 (0.001)
All	16.674 (0.060)	NA

Vassiliev invariant of the second degree. We select such polygons that have the same set of values of the two knot invariants. Here we calculate $v_2(K)$ by the algorithm given in [30]. The two knot invariants are practically useful for computer simulation of random polygons with a large number of polygonal nodes [31].

We consider four different topological classes: the trivial knot (0), the trefoil knot (3_1), the figure-eight knot (4_1), and the other knots (*other*). We denote by "*all*" such polygons that have no topological constraint.

Let us denote by $\langle R^2_{G,K}\rangle$ the mean-square radius of gyration of Gaussian random polygons with N nodes under a given topological constraint K. The estimates of $\langle R^2_{G,K}\rangle$ for $N=200$ are given in Table I for several knots. We find in Table I that for $N=200$, the trivial knot ($K=0$) is the largest and the trefoil knot ($K=3_1$) is almost equal to but slightly less than the average ($K=all$), while the figure-eight knot ($K=4_1$) and other knots ($K=other$) are smaller than the average ($K=all$). Thus, the estimates of $\langle R^2_{G,K}\rangle$ for the five topological conditions are given in increasing order as follows:

$$R^2_{G,0} > R^2_{G,all} > R^2_{G,3_1} > R^2_{G,4_1} > R_{G,other}. \tag{7}$$

The fractions of such Gaussian polygons of $N=200$ that have given knot types among the 10^5 generated polygons are shown in Table I for the different topological conditions. The fraction of the trivial knot is given by about 0.53, which gives the largest one. The fraction of the trefoil knot is given by about 0.21, and it is the most dominant nontrivial knot for $N=200$.

For different numbers of N, the estimates of $\langle R^2_{G,K}\rangle$ have been obtained in Ref. [10]. The fraction of Gaussian polygons with a given knot has also been evaluated for some species of knots [32].

III. RADIAL DISTRIBUTION FUNCTIONS

A. Probability distribution $4\pi r^2 g_K(r)\Delta r/N$

Let us recall definition (1) of the segment pair correlation function of a polymer with N segments. The correlation function $g(\boldsymbol{r})$ depends only on the distance $r=|\boldsymbol{r}|$ due to the rotational symmetry. We denote it by $g(r)$ and call it the radial distribution function. Here we note that $4\pi r^2 g(r)\Delta r/N$ gives the probability of other segments appearing in a spherical shell from radius r to $r+\Delta r$ centered at a given segment.

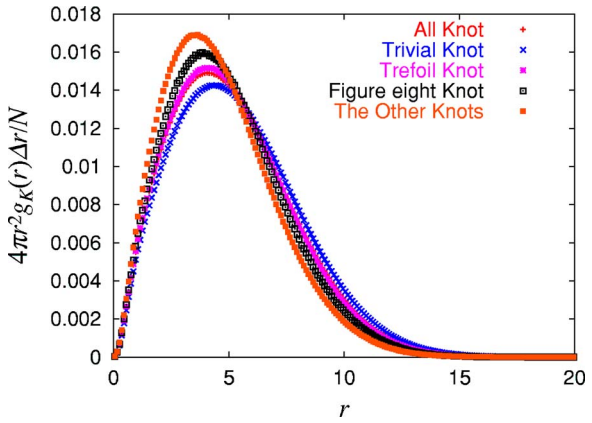

FIG. 1. (Color online) The probability distribution $4\pi r^2 g_K(r)\Delta r/N$ versus the distance r. Here $N=200$ and $\Delta r=0.1$. The plots of the five topological conditions, *all*, 0, 3_1, 4_1, and *other*, are represented by crosses, tilted crosses, double crosses, open squares, and closed squares, respectively.

For a Gaussian polygon under a topological condition K, we denote by $g_K(\boldsymbol{r})$ and $g_K(r)$ the pair correlation function and the radial distribution function, respectively. The graphs of the probability distribution $4\pi r^2 g_K(r)\Delta r/N$ are plotted against r in Fig. 1. They are consistent with a preliminary result [22].

B. Gyration radius $R_{G,K}$ as the peak position of the probability distribution $4\pi r^2 g_K(r)\Delta r/N$

Recently, it has been observed [33] that for a random polygon under no topological constraint, the peak position of the probability distribution $4\pi r^2 g(r)\Delta/N$ should be given by the gyration radius of the random polygon. We shall show that the new observation is valid also in the case of random polygons under topological constraints.

Let us consider the Gaussian random polygon of $N=200$. The estimates of the peak position of the probability distribution $4\pi r^2 g_K(r)\Delta r/N$ for the five topological conditions are listed in Table II together with those of the gyration radius $R_{G,K}$. Here we recall that $R_{G,K}$ denotes the square root of the mean-square radius of gyration—i.e., $R_{G,K}=\sqrt{\langle R^2_{G,K}\rangle}$. The peak position r_{peak} and the gyration radius $R_{G,K}$ are almost identical up to numerical errors in Table II. Thus, the equivalence $r_{\text{peak}}=R_{G,K}$ has been numerically established within er-

TABLE II. Peak position r_{peak} of the probability distribution $4\pi r^2 g_K(r)\Delta r/N$ for a topological condition K. The estimates of r_{peak} may have errors of order 0.1 at most.

K	r_{peak}	$R_{G,K}$
0	4.25	4.246
3_1	4.05	4.026
4_1	3.85	3.879
Other	3.65	3.669
All	4.05	4.083

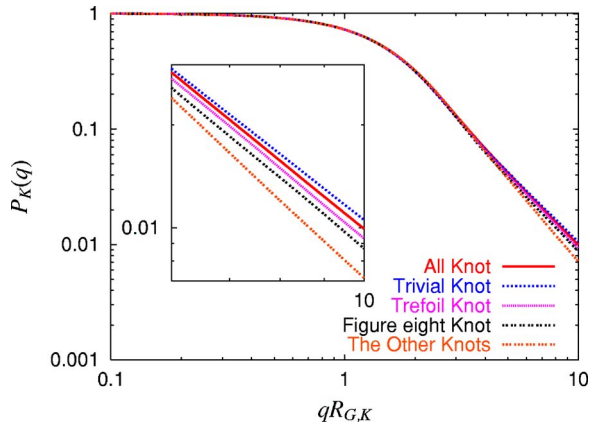

FIG. 2. (Color online) Double-logarithmic plot of the form factor $P_K(q)$ of an N-noded Gaussian polygon under a topological condition K versus the variable $u=qR_{G,K}$. The curves colored with red (solid), blue (dotted), purple (continually dotted), black (dotted dimers), and orange (dotted trimers) correspond to the cases of no topological condition (*all*), the trivial knot (0), the trefoil knot (3_1), the figure-eight knot (4_1), and the other knots (*other*), respectively. In the inset, the main panel is enlarged from $qR_{G,K}=6$ to 10; the graphs of 0, *all*, 3_1, 4_1, and *other* are located from higher to lower positions.

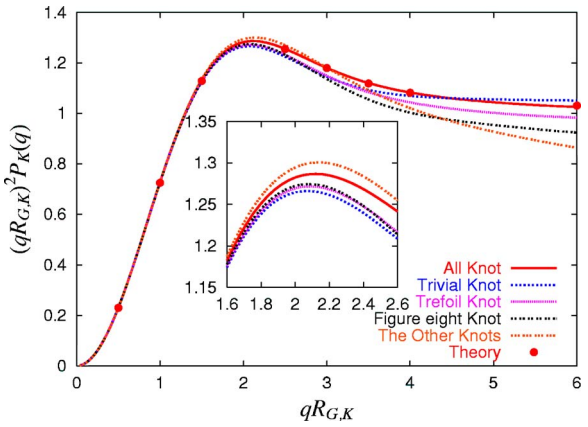

FIG. 3. (Color online) Plot of $(qR_{G,K})^2P_K(q)$ versus $u=qR_{G,K}$. The Kratky plots of the trivial, trefoil, and figure-eight knots are represented by the blue (dotted), purple (continually dotted), and black (dotted with dimers) curves, respectively. The red (solid) curve corresponds to the case of no topological constraint. In the inset, the graphs near peak positions are enlarged. The red dots are calculated by using the analytical expression of the scattering function of ring polymers given by Casassa [1].

rors. The equivalence should be characteristic to ring polymers. In fact, for a Gaussian linear chain, the peak position of the probability distribution $4\pi r^2 g(r)\Delta r/N$ is located at $r \approx 0.74R_{G,lin}$, where $R_{G,lin}$ denotes the square root of the mean-square radius of gyration for the linear chain [17].

IV. SCATTERING FUNCTIONS

A. Form factor of a knotted random polygon

Let us recall definition (2) of the scattering function $g(\boldsymbol{q})$ for a polymer with N segments. The scattering function $g(\boldsymbol{q})$ depends only on $q=|\boldsymbol{q}|$, due to rotation symmetry. We denote it by $g(q)$. For a Gaussian polygon under a topological condition K, we denote the scattering function by the symbol $g_K(q)$.

We define the form factor $P_K(q)$ for a Gaussian polygon under a topological condition K as follows:

$$P_K(q) = \frac{g_K(q)}{g_K(0)}. \tag{8}$$

We have $P_K(q)=g_K(q)/N$ from definition (2). Let us define variable u by $u=qR_{G,K}$. Here we recall that $R_{G,K}$ denotes the square root of the mean-square radius of gyration for the Gaussian random polygon under a given topological constraint K. Similarly as Eq. (4), we define f_K, a function of variable u, by $P_K(q)=f_K(qR_{G,K})$.

The double-logarithmic plot of the form factor $P_K(q)$ versus $u=qR_{G,K}$ [i.e., $f_K(u)$ versus u] is shown in Fig. 2. Here we recall that the form factor $P_{all}(q)$ was evaluated analytically in terms of the Dawson integral [1]. In Fig. 2 we have evaluated the form factor $P_K(q)$ for the five topological conditions through simulation.

In the region from $u=0$ up to $u=2$ or 3, the form factors $P_K(q)$ for the five topological conditions overlap each other in the double-logarithmic scales. We note that the low-q part of the form factor $P_K(q)$ is related to the large-r part of the radial distribution function $g_K(r)$ through the Fourier transformation. We shall show the correspondence precisely through the Kratky plot in Fig. 3.

For $u>5$, the graphs of the different topological conditions make approximately straight lines in the main panel. In the inset of Fig. 2, the graphs, except for those of the other knots (*other*), make distinct lines parallel to each other. The gradient is almost given by -2, which is consistent with the Gaussian asymptotic behavior.

It follows from the four parallel and distinct lines in the inset of Fig. 2 that for large q the form factor $P_K(q)=f_K(qR_{G,K})$ is approximated by

$$f_K(u) \approx a_K/u^2, \tag{9}$$

where the constants a_K are distinct for the four topological conditions. They are given in increasing order as follows: $a_0 > a_{all} > a_{3_1} > a_{4_1}$. Here, the estimates of a_K for $K=0, 3_1, 4_1$, *other*, and *all* are given by 1.05, 0.97, 0.91, 0.84, and 1.01, respectively. It is suggested from the estimates of a_K that with the monomer number N fixed, the asymptotic constant value a_K should be smaller when the knot K is more complex.

B. Kratky plot for a knotted random polygon

Let us discuss the Kratky plots of the form factors $P_K(q)$ for some different topological conditions. The plots of $(qR_{G,K})^2P_K(q)$ versus the variable $u=qR_{G,K}$ are shown in Fig. 3. In other words, they are the plots of $u^2f_K(u)$ versus u for the different topological conditions K. Here we have numerically evaluated the Fourier transformations of the radial dis-

TABLE III. Peak position u_{peak} of the Kratky plot $(qR_{G,K})^2P_K(q)$ versus $u=qR_{G,K}$ for the Gaussian random polygon under a given topological condition K. The q value is given by an integral multiple of 0.01.

K	u_{peak}	Peak height
0	2.08	1.266
3_1	2.09	1.272
4_1	2.09	1.275
Other	2.09	1.300
All	2.08	1.287

tribution functions by an interpolation method [33].

With the graphs shown in Fig. 3 we observe that the mean-square radius of gyration, $\langle R_{G,K}^2\rangle$, plays an important role in the scattering function of the Gaussian polygon under a topological condition K. In fact, plotting the form factor in terms of variable u makes the graphs quite simple. In particular, in the small-u region such as $u<2$, the Kratky plots for the different topological conditions overlap completely. For $u>2$ the graphs become separate gradually.

The peak positions of the Kratky plots are given by almost the same value of u for all the five topological conditions. The estimates of the peak positions are given in Table III. They are the same value with respect to errors.

The peak heights of the Kratky plots depend on the topological conditions, as shown in the inset of Fig. 3. The estimates of the peak height are also listed in Table III. The Kratky plot for the trivial knot has the smallest peak height. The peak height for the trefoil knot is a little larger than that of the trivial knot. However, for the Kratky plots of the trefoil and figure-eight knots, the peak heights are given by almost the same value.

The Kratky plots of Fig. 3 are not in contradiction with those of the previous studies, and even generalize them. For lattice random polygons with $N=160$, the Kratky plots were numerically evaluated for all polygons and knotted polygons, respectively [6]. We note in Table I that the majority of polygons with nontrivial knots are given by those of the trefoil knot for the Gaussian polygons with $N=200$. Thus, the Kratky plots of all polygons and knotted polygons shown in Ref. [6] approximately correspond to the plots of no topological constraint and the trefoil knot, respectively, which are shown in Fig. 3.

C. Small-q behavior

Let us discuss the observation that the plots of $u^2f_K(u)$ versus u for the different topological conditions overlap completely in the region of $u<2$. Here we recall that the variable u is the wave number q normalized by $R_{G,K}$. We have

$$f_K(u)=f_{all}(u) \quad \text{for } u<2. \tag{10}$$

The observation suggests that the large-r behavior of the radial distribution function $g_K(r)$ is given by rescaling the function with the gyration radius $R_{G,K}$. Here we note that the large-r part of $g_K(r)$ is related to the small-q part of $P_K(q)$ through the Fourier transformation.

In terms of the form factor, we have from Eq. (10) the following:

$$P_K(q)=f_{all}(qR_{G,K}) \quad \text{for } q<2/R_{G,K}. \tag{11}$$

Thus, the small-q part of the form factor $P_K(q)$ is essentially given by that of the Gaussian random polygon under no topological constraint. The knot dependence is simply renormalized by the average size—i.e., $R_{G,K}$. Here we note the exact correspondence

$$u^2f_K(u)du=R_{G,K}^3q^2P_K(q)dq, \tag{12}$$

where $u=qR_{G,K}$.

The numerical result (11) should be consistent with the observation that in the small-q region, the scattering function of a polymer should depend only on the average size of the polymer. In fact, the Kratky plot of a spherical molecule overlap with that of a rodlike molecule in some small-u region [17]. Here we remark that it should be interesting to discuss the numerical result (11) from the viewpoint of local knots [18]. However, it is not clear how the present numerical result is related to local knots or not. We should discuss it in future simulation studies.

D. Large-q behavior

For $u>5$, we observe that each of the Kratky plots of Fig. 3 approaches a constant value in the large-u limit. We thus suggest an asymptotic behavior that for any topological constraint K the form factor $P_K(q)$ should become close to that of the Gaussian polygon for $u\gg 1$, such as $P_K(q)\propto 1/(qR_{G,all})^2$. Here we recall that when $u\gg 1$ the form factor $P_{lin}(q)$ of a Gaussian linear chain is approximated by $P_{lin}(q)\approx 2/(qR_{G,lin})^2$.

In the double-logarithmic plot of Fig. 2 the large-q behavior of the form factor is given by $P_K(q)\approx a_K/(qR_{G,K})^2$. We thus have

$$(qR_{G,K})^2P_K(q)\approx a_K \quad \text{for } q\gg 1/R_{G,K.} \tag{13}$$

As we have discussed with Eq. (9), the asymptotic constant values a_K for the four topological conditions 0, all, 3_1, and 4_1 are given in increasing order as $a_0>a_{all}>a_{3_1}>a_{4_1}$, which is the same with the order among the values $\langle R_{G,K}^2\rangle$ given in Table I.

Through the observation in the above we may suggest that if knot K becomes more complex, the average spatial configuration of random polygons with fixed knot K should become closer to that of spherical molecules than that of rod like molecules. Here we recall that in the large-q region, the form factor of a spherical molecule has much smaller values than that of a rod like molecule [17]. With the same number of monomers given, the spherical molecule is much more compact and smaller in size than the rod like molecule. The spherical one has a much smaller value of the mean-square radius of gyration. Thus, we suggest that the spatial configuration of a random polygon with a more complex knot should be more spherical than that of a less complex knot. In

fact, it is consistent with the observations that as knot K becomes more complex the Kratky plot for knot K becomes smaller in the large-q region and the value of $R_{G,K}$ is given by a smaller value.

The estimates of a_K are roughly consistent with the values of the Kratky plots at $u=6$ for the four topological conditions except for the case of *other*. Here we note that for $u>10$, systematic errors of the Kratky plots could be larger than statistical errors of the gyration radius $R_{G,K}$. Thus, we have limited the Kratky plot up to $u=6$ in Fig. 3. In the region of $u<6$, the Kratky plot for $K=all$ obtained in the simulation overlaps with the theoretical points obtained by the exact expression derived by Casassa [1], as seen in Fig. 3.

Finally we recall that the distribution function between opposite nodes of a random polygon with a fixed knot was evaluated through a simulation recently, and it was found to be close to the Gaussian one [28]. The interpretation (13) should be consistent also with the observation.

[1] E. F. Casassa, J. Polym. Sci., Part A: Gen. Pap. **3**, 605 (1965).
[2] A. V. Vologodskii, A. V. Lukashin, M. D. Frank-Kamenetskii, and V. V. Anshelevich, Sov. Phys. JETP **39**, 1059 (1974).
[3] J. R. Roovers and P. M. Toporowski, Macromolecules **16**, 843 (1983).
[4] *Cyclic Polymers*, 2nd ed., edited by J. A. Semlyen (Kluwer Academic, Dordrecht, 2000).
[5] W. Burchard, in *Cyclic Polymers* [4], pp. 43–84.
[6] G. ten Brinke and G. Hadziioannou, Macromolecules **20**, 480 (1987).
[7] J. des Cloizeaux, J. Phys. (France) Lett. **42**, L433 (1981).
[8] J. M. Deutsch, Phys. Rev. E **59**, R2539 (1999).
[9] A. Yu. Grosberg, Phys. Rev. Lett. **85**, 3858 (2000).
[10] M. K. Shimamura and T. Deguchi, J. Phys. A **35**, L241 (2002).
[11] A. Dobay, J. Dubochet, K. Millett, P. E. Sottas, and A. Stasiak, Proc. Natl. Acad. Sci. U.S.A. **100**, 5611 (2003).
[12] H. Matsuda, A. Yao, H. Tsukahara, T. Deguchi, K. Furuta, and T. Inami, Phys. Rev. E **68**, 011102 (2003).
[13] N. T. Moore, R. C. Lua, and A. Y. Grosberg, Proc. Natl. Acad. Sci. U.S.A. **101**, 13431 (2004).
[14] M. K. Shimamura and T. Deguchi, Phys. Rev. E **64**, 020801(R) (2001).
[15] M. K. Shimamura and T. Deguchi, Phys. Rev. E **65**, 051802 (2002).
[16] M. Doi, *Introduction to Polymer Physics* (Clarendon Press, Oxford, 1996).
[17] I. Teraoka, *Polymer Solutions* (Wiley, New York, 2002).
[18] B. Marcone, E. Orlandini, A. L. Stella, and F. Zonta, J. Phys. A **38** L15 (2005).
[19] R. Metzler, A. Hanke, P. G. Dommersnes, Y. Kantor, and M. Kardar, Phys. Rev. Lett. **88** 188101 (2002).
[20] O. Farago, Y. Kantor, and M. Kardar, Europhys. Lett. **60**, 53 (2002).
[21] R. Zhandi, Y. Kantor, and M. Kardar, ARI The Bulletin of the ITU **53**, 6 (2003).
[22] M. K. Shimamura and T. Deguchi, in *Physical and Numerical Models in Knot Theory*, edited by J. A. Calvo, K. C. Millett, and E. J. Rawdon (World Scientific, Singapore, 2005), pp. 399–419.
[23] K. V. Klenin, A. V. Vologodskii, V. V. Anshelevich, A. M. Dykhne, and M. D. Frank-Kamenetskii, J. Biomol. Struct. Dyn. **5**, 1173 (1988).
[24] E. J. Janse van Rensburg and S. G. Whittington, J. Phys. A **24**, 3935 (1991).
[25] E. Orlandini, M. C. Tesi, E. J. Janse van Rensburg, and S. G. Whittington, J. Phys. A **31**, 5953 (1998).
[26] M. K. Shimamura and T. Deguchi, Phys. Lett. A **274**, 184 (2000).
[27] M. K. Shimamura and T. Deguchi, J. Phys. Soc. Jpn. **70**, 1523 (2001).
[28] A. Yao, H. Tsukahara, T. Deguchi, and T. Inami, J. Phys. A **37**, 7993 (2004).
[29] J. des Cloizeaux and M. L. Mehta, J. Phys. (Paris) **40**, 665 (1979).
[30] M. Polyak and O. Viro, Int. Math. Res. Notices No. 11, 445 (1994).
[31] T. Deguchi and K. Tsurusaki, Phys. Lett. A **174**, 29 (1993).
[32] T. Deguchi and K. Tsurusaki, Phys. Rev. E **55**, 6245 (1997).
[33] K. Kamata, Master thesis (in Japanese), Ochanomizu University, 2005.